

Electronic structure of the Fe²⁺ compound FeWO₄: A combined experimental and theoretical x-ray photoelectron spectroscopy study

S. G. Altendorf¹, D. Takegami¹, A. Meléndez-Sans¹, C. F. Chang¹, M. Yoshimura², K. D. Tsuei², A. Tanaka³, M. Schmidt¹ and L. H. Tjeng¹

¹Max Planck Institute for Chemical Physics of Solids (MPI-CPfS), Nöthnitzer Straße 40, 01187 Dresden, Germany

²National Synchrotron Radiation Research Center (NSRRC), Hsinchu 30076, Taiwan

³Department of Quantum Matter, Hiroshima University, Higashi-Hiroshima 739-8530, Japan



(Received 26 June 2023; accepted 27 July 2023; published 16 August 2023)

The electronic structure of FeWO₄ is studied by photoelectron spectroscopy at x-ray and hard x-ray photon energies on high-quality single crystals. Photoionization cross-section effects together with full atomic multiplet configuration interaction and band structure calculations allow us to identify the contributions of iron and tungsten to the valence band. The analysis shows that the correlations in FeWO₄ necessitate theoretical approaches beyond standard band structure models even for the description of the tungsten with a formal 5d⁰ configuration.

DOI: [10.1103/PhysRevB.108.085119](https://doi.org/10.1103/PhysRevB.108.085119)

I. INTRODUCTION

Transition metal tungstates have attracted the attention of the research community due to their remarkable electrochemical and catalytic properties. A large variety of potential technological applications such as photocatalysts, photoanodes in water splitting reactions, electrodes in batteries, supercapacitors, electrochromic devices, and gas sensors are discussed [1–9].

In this work we focus on the iron tungstate (FeWO₄). The semiconducting antiferromagnet has a band gap of about 2 eV [10] and a Neel temperature of 75 K [11–14]. It belongs to the wolframite-type tungstates that crystallize in a monoclinic structure in which the iron and tungsten atoms are both surrounded by six oxygen atoms. These octahedral FeO₆ and WO₆ clusters form two edge-shared zigzag chains along the [001] direction [14,15].

The observed large electrochemical activity of FeWO₄ has been assigned to reversible Fe²⁺/Fe³⁺ surface redox reactions [4], making especially samples with large surface area attractive for applications. Therefore, most reported studies have been performed on various forms of nanocrystals, nanostructures, or polycrystalline materials. Detailed studies on the electronic structure of monophase FeWO₄ single crystals are still lacking for a fundamental understanding of the intrinsic properties. Having recently established the synthesis of millimeter-size high-quality single crystals [14], we present here a thorough investigation of the electronic structure of FeWO₄ that combines experimental photoelectron spectroscopy at different photon energies and theory.

II. METHODS

FeWO₄ single crystals were prepared by chemical transport reaction as described in detail previously [14]. The electronic structure of the samples was experimentally studied by x-ray photoelectron spectroscopy at various photon energies to make use of the different photoionization cross sections of the constituents. The hard x-ray photoelectron spectroscopy (HAXPES) data were collected at the Max-Planck-NSRRC HAXPES end station at the Taiwan undulator beamline BL12XU at SPring-8, Japan. The photon energy was set to about 6.5 keV and the light was linearly polarized with the electrical field vector in the horizontal plane. The photoelectrons were collected using a horizontally mounted MB Scientific A-1 HE analyzer [16]. The x-ray photoelectron spectroscopy (XPS) data were taken in the laboratory at the MPI-CPfS in Dresden using Vacuum Generators twin crystal monochromatized Al K_α light (1486.6-eV photons) and a Scienta R3000 electron energy analyzer. The Fermi levels and the energy resolutions were calibrated using Au or Ag references. The overall energy resolution was ≈0.3 eV for HAXPES and ≈0.4 eV for XPS. All measurements were performed in near-normal emission geometry and at room temperature. The FeWO₄ crystals were cleaved and measured under ultrahigh vacuum conditions (low 10⁻¹⁰ mbar range) guaranteeing a high surface quality.

To model the iron contribution to the valence band region of the photoelectron spectra, we carried out full atomic multiplet configuration-interaction-based cluster calculations [17–19]. The calculations were performed for an FeO₆ cluster in octahedral coordination using the XTLS code (version 9.25) [19]. For comparison with the experimental results, a combination of Gaussian and Lorentzian broadening was applied.

Density functional theory calculations within the local density approximation were performed to derive the band structure of the material. The full-potential local-orbital code FPLO (version 18.00-52) [20] was employed using the

Published by the American Physical Society under the terms of the [Creative Commons Attribution 4.0 International](https://creativecommons.org/licenses/by/4.0/) license. Further distribution of this work must maintain attribution to the author(s) and the published article's title, journal citation, and DOI. Open access publication funded by the Max Planck Society.

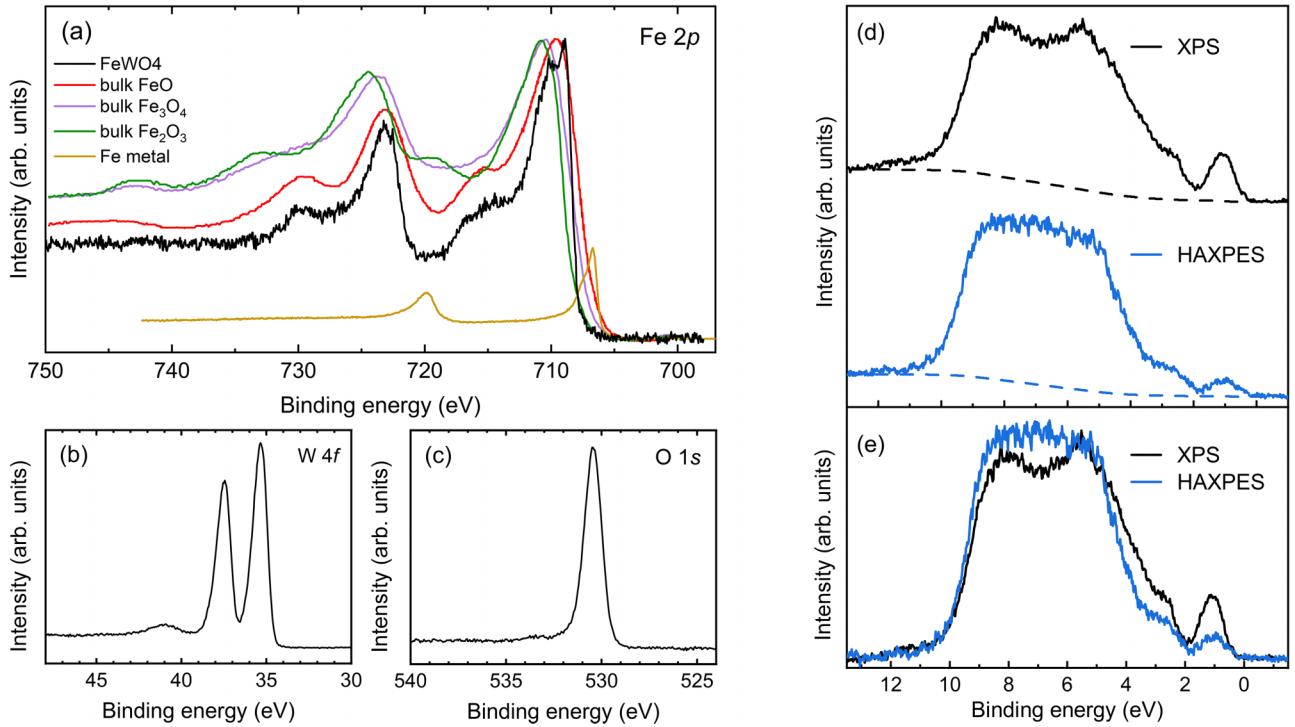


FIG. 1. Photoelectron spectra of an FeWO_4 single crystal. [(a)–(c)] $\text{Fe } 2p$ with references (Fe metal film [22], Fe_2O_3 [23], Fe_3O_4 [23], and FeO [23]), $\text{W } 4f$, and $\text{O } 1s$ XPS core levels, respectively. [(d),(e)] Valence band (VB) taken at photon energies of 1486.6 eV (XPS, black) and 6.5 keV (HAXPES, blue). (d) Spectra with corresponding integral background. (e) Comparison of the spectra that are normalized to the area after subtraction of the integral background.

exchange and correlation potential of Perdew and Wang [21] and a full relativistic, nonmagnetic approach.

III. RESULTS

To determine the valence states of iron and tungsten in the FeWO_4 single crystal, we performed core-level XPS measurements. Figures 1(a)–1(c) show the $\text{Fe } 2p$, $\text{W } 4f$, and $\text{O } 1s$ spectra, respectively. For the $\text{Fe } 2p$ spectra, we include also reference spectra of Fe metal [22], Fe_2O_3 [23] (Fe^{3+}), Fe_3O_4 [23] (Fe^{2+} and Fe^{3+}), and FeO [23] (mainly Fe^{2+}). A comparison to the energy positions of the spectral features reveals that the iron in FeWO_4 has a clean 2+ valence. The $\text{W } 4f$ states have a pronounced double-peak structure whose shape and energy position are characteristic for a pure W^{6+} valence. A detailed discussion on the tungsten valence can be found in our previous work [14], which refers to a photoemission measurement on the same FeWO_4 crystal and gives a quantitative estimate on the level of accuracy ($<1\%$ W^{5+}). For completeness, also the $\text{O } 1s$ level is shown which exhibits a symmetric single peak indicative of a high-quality oxide crystal without any significant amount of defects or contamination.

We would like to note that from a chemical perspective the coexistence of Fe^{2+} and W^{6+} is not trivial. In most oxide compounds, the iron does not have a pure Fe^{2+} valence. Usually at least some contribution of Fe^{3+} is observed. One example is FeO which is thermodynamically unstable and readily forms the Fe-deficient compound $\text{Fe}_{1-\delta}\text{O}$ [24]. The Fe^{3+} contribution leads to a broadening of the $\text{Fe } 2p$ spectrum [cf. bulk FeO reference (red curve) in Fig. 1(a)]. In contrast,

FeWO_4 has significantly sharper $\text{Fe } 2p$ features, revealing a very pure Fe^{2+} valence. The XPS results confirm the high quality of the FeWO_4 crystals with clean W^{6+} and Fe^{2+} oxidation states in agreement with recent findings by x-ray absorption spectroscopy on crystals of the same batch [14]. These results show that FeWO_4 can also serve as a Fe^{2+} standard for spectroscopic measurements.

In Figs. 1(d) and 1(e), the valence band spectra measured at photon energies of 1486.6 eV (XPS) and 6.5 keV (HAXPES) are shown. They consist of a distinct peak close to the Fermi level at around 1 eV binding energy, which is well separated from a region of larger intensity between 2 and 10 eV. The direct comparison of the background-corrected and normalized spectra in Fig. 1(e) illustrates the differences. Part of the spectral weight shifts from lower (0–5 eV) to higher (5–10 eV) binding energies when going from XPS to HAXPES photon energies. This photon energy dependence reveals that different ionization cross sections are involved, suggesting that more than one constituent contributes to the valence band.

In the following, we investigate in detail the composition of the valence band spectrum to gain a better understanding of the electronic structure of FeWO_4 . We start with general considerations from a theoretical point of view: Fe^{2+} has a $3d^6$ configuration and is known to be highly correlated. Therefore, configuration-interaction-based cluster calculations might be a suitable method to derive the contribution of the iron. Contrarily, W^{6+} has a $5d^0$ configuration. Given the empty $5d$ shell, one might expect a more bandlike character of the tungsten, which then could be adequately described by band structure calculations.

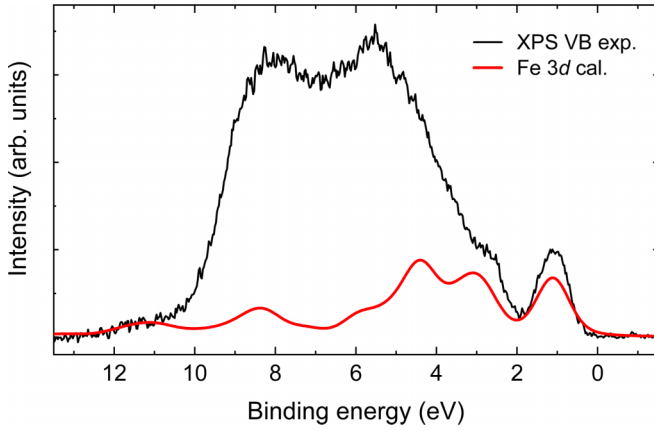


FIG. 2. Comparison of the calculated Fe 3d photoelectron spectrum and the experimental XPS valence band spectrum. The iron contribution was theoretically derived from a configuration-interaction-based cluster model for an FeO₆ octahedron using the parameter values given in Ref. [25]. The calculated spectrum was shifted in energy to match the experimental data.

First, we consider the contribution of the iron. The Fe²⁺ ions in the FeWO₄ crystal are locally surrounded by six oxygen ions. We approximate the structure by an FeO₆ cluster with octahedral symmetry for which we perform full atomic multiplet configuration-interaction-based calculations. The parameters typically used to model Fe²⁺ systems, for instance, for FeO ($U_{dd} = 6$ eV, $\Delta = 7$ eV [19]; $U_{dd} = 7$ eV, $\Delta = 6$ eV [26]) or for an Fe²⁺ impurity in MgO ($U_{dd} = 6$ eV, $\Delta = 7.5$ eV) [27], had to be adapted slightly to match the experimental FeWO₄ results ($U_{dd} = 5$ eV, $\Delta = 8$ eV). The full list of parameters is given in Ref. [25].

Figure 2 shows the corresponding calculated Fe 3d photoelectron spectrum together with the measured XPS valence band. A comparison of experiment and theory immediately indicates that the peak at 1 eV binding energy is related to the iron. In fact, this low-energy feature is observed also for other Fe²⁺-containing compounds like Fe₃O₄ [28]. It is a signature of the Fe²⁺ 3d⁶ high-spin configuration and can be assigned to the photoemission of the minority spin electron of the 3d⁶ shell (3d⁶ → 3d⁵ transition with ⁶A₁ final state) [28,29]. This is very different from Fe³⁺ compounds with pure Fe 3d⁵ configurations which have a larger band gap and do not show a comparable feature close to the Fermi level, such as, e.g., Fe₂O₃ [30]. Thus, the absence of such a low-energy feature in Fe²⁺ materials can be an indication of a poor quality or degradation of the investigated sample.

We note that the calculated Fe²⁺ spectrum has striking similarities with the calculated spectrum of the Co³⁺ high-spin state which has the same 3d⁶ high-spin electron configuration (cf. Refs. [31,32]).

To include also the other constituents of the FeWO₄ in our analysis, we perform band structure calculations. Figure 3(a) shows the calculated total density of states (DOS) together with the partial densities of states of the elemental subshells that have a significant contribution to the valence band, namely, Fe 3d, W 5d, and O 2p. Similar to the experiment, the calculations show a broad spectral feature between

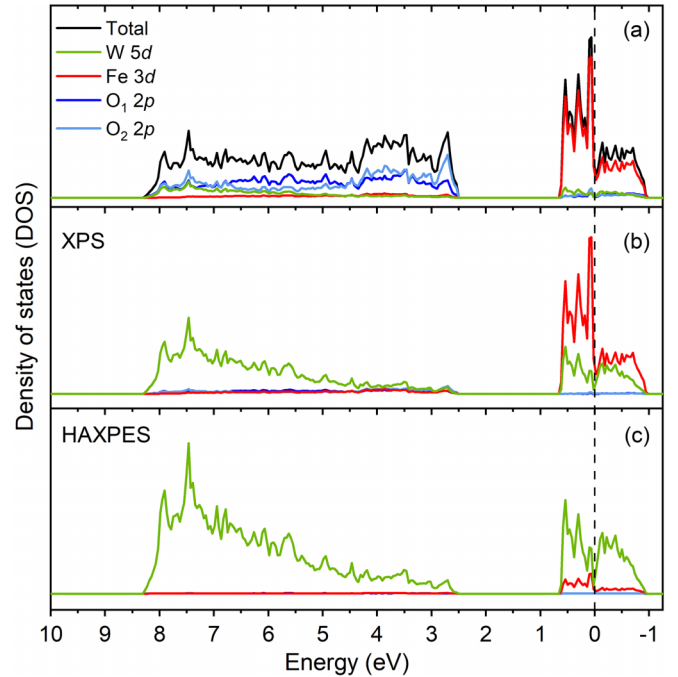


FIG. 3. Band structure calculations for FeWO₄. (a) The total density of states and the partial densities of states of the atomic subshells that are relevant for the valence band, namely, W 5d, Fe 3d, and O 2p for the two oxygen sites, are shown. The Fermi level is at zero energy. To compare the calculations with the experiment, the partial densities of states are multiplied by the photoionization cross sections for the XPS (b) and the HAXPES (c) energies which are listed in Table I.

about 2.5 and 8.5 eV. Furthermore, there is an intense peak structure around zero energy. In contrast to the measurement, no band gap is opened. This is not unexpected since the calculations are performed without on-site Coulomb repulsion (U) and magnetic ordering. When taking a closer look at the band structure results, we observe that where iron is present there is also a contribution from tungsten, and where tungsten is present there is also a contribution from iron, indicating a non-negligible hybridization between the two elements mediated by the oxygens.

For a comparison with the experiments, the photoionization cross sections for the different subshells have to be considered. The relevant values are listed in Table I. According to the band structure calculations, the intensity (I) of the valence band spectra are almost exclusively built up from Fe 3d, W 5d, and O 2p. Following the approach of Ref. [33], we can then formulate two equations for the spectra taken at XPS (XP) and HAXPES (HP) photon energies weighting the partial densities of states (ρ) by the respective photoionization cross sections (σ):

$$I_{XP} = c_{XP} (\sigma_{XP}^{Fe3d} \rho^{Fe3d} + \sigma_{XP}^{W5d} \rho^{W5d} + \sigma_{XP}^{O2p} \rho^{O2p}), \quad (1)$$

$$I_{HP} = c_{HP} (\sigma_{HP}^{Fe3d} \rho^{Fe3d} + \sigma_{HP}^{W5d} \rho^{W5d} + \sigma_{HP}^{O2p} \rho^{O2p}). \quad (2)$$

The proportionality factors c_{XP} and c_{HP} are included to correct for experimental uncertainties, such as the unknown absolute values of photon flux and transmission efficiency of the analyzer.

TABLE I. Photoionization cross sections (σ) for the atomic subshells that contribute to the valence band of FeWO_4 for 1486.6-eV and 6.5-keV photon energies. The values are extrapolated from the cross-section tables in Refs. [34–36] and divided by the number of electrons in the completely filled subshell. The cross-section values for 6.5 keV are corrected to account for the linear polarized light and the horizontal geometry of the experiment (see Refs. [16,34–37]).

	XPS 1486.6 eV σ/e^- (kb)	HAXPES 6.5 keV corr. σ/e^- (kb)
W 5d	1.495	0.0916
Fe 3d	0.355	0.0014
O 2p	0.060	0.0002

Figures 3(b) and 3(c) show the calculated partial densities of states weighted by the photoionization cross sections. While the valence band for the XPS photon energy consists of contributions of W 5d and Fe 3d, the HAXPES spectrum is nearly exclusively dominated by the W 5d states. The oxygen contribution is small for both photon energies. Thus, we can neglect the last terms of Eqs. (1) and (2), and the following relations can be derived for the Fe 3d and W 5d densities of states, which allow us to extract the contributions of iron and tungsten to the valence band from the experimental results:

$$\rho^{\text{Fe}3d} \sim I_{\text{XP}} - A \times I_{\text{HP}}, \quad (3)$$

$$\rho^{\text{W}5d} \sim I_{\text{HP}} - B \times I_{\text{XP}}, \quad (4)$$

with parameters $A = \frac{c_{\text{XP}}}{c_{\text{HP}}} \times \frac{\sigma_{\text{XP}}^{\text{W}5d}}{\sigma_{\text{HP}}^{\text{W}5d}}$ and $B = \frac{c_{\text{HP}}}{c_{\text{XP}}} \times \frac{\sigma_{\text{HP}}^{\text{Fe}3d}}{\sigma_{\text{XP}}^{\text{Fe}3d}}$.

Since the proportionality factors c_{HP} and c_{XP} are difficult to determine experimentally, we focus on the product $A \times B$ which can be readily calculated from the cross-section values listed in Table I:

$$A \times B = \frac{\sigma_{\text{XP}}^{\text{W}5d}}{\sigma_{\text{HP}}^{\text{W}5d}} \times \frac{\sigma_{\text{HP}}^{\text{Fe}3d}}{\sigma_{\text{XP}}^{\text{Fe}3d}} = 0.064. \quad (5)$$

Following Eq. (3), the contribution of the iron can be extracted from the differences in the XPS and HAXPES valence band spectra, which we then compare to the results of the configuration-interaction-based cluster calculation. Figure 4(a) shows the experimental spectra and their difference curve. The scaling factor A is chosen such that the difference curve (light red) matches the shape of the iron contribution obtained from the cluster calculations (dark red). Indeed for $A = 0.8$, the difference curve resembles the shape of the theoretical spectrum quite well over the entire range of the measurement.

Having deduced that $A = 0.8$, we can calculate from Eq. (5) that $B = 0.08$. According to Eq. (4), the difference of the HAXPES spectrum and the scaled XPS spectrum should resemble the tungsten contribution to the valence band. A comparison of the difference spectrum (light green) with the W 5d density of states from band structure calculations (dark green), however, shows significant deviations, as can be seen in Fig. 4(b). The band structure calculation yields a larger intensity at 1 eV binding energy while spectral weight is missing between 3 and 7 eV. The intensity of the low-energy feature is related to the hybridization between tungsten and iron. Its

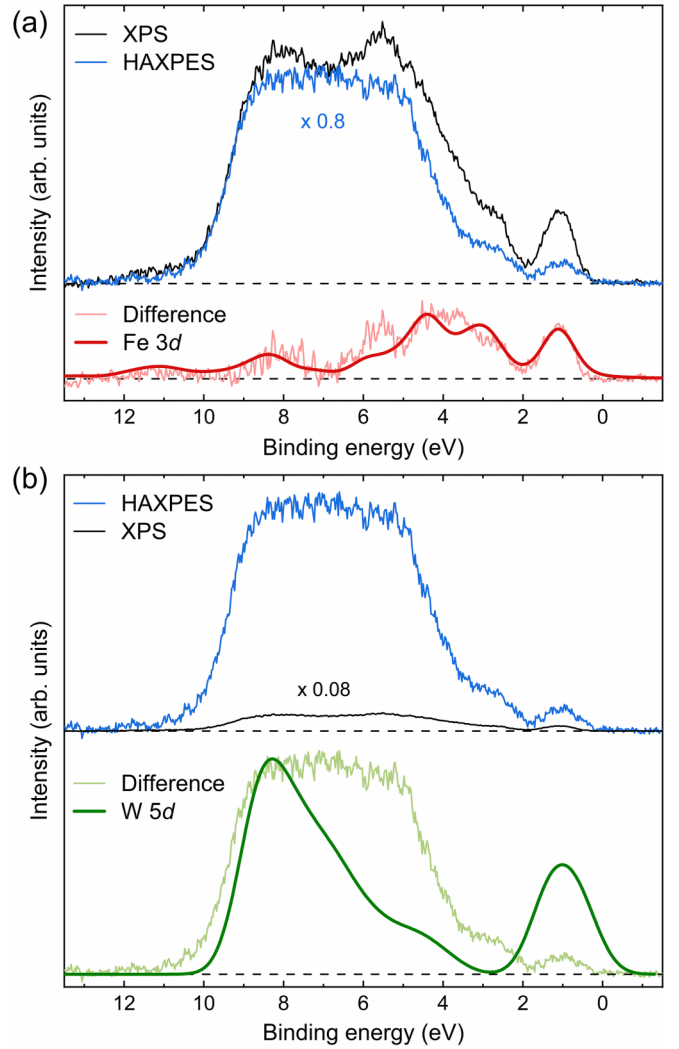


FIG. 4. Fe 3d and W 5d densities of states deduced from the normalized and background-corrected valence band spectra taken at XPS and HAXPES photon energies following Eqs. (3) and (4). (a) Iron contribution. The HAXPES spectrum has been rescaled by a factor of $A = 0.8$. The difference spectrum is compared to the results of the configuration-interaction-based cluster calculation. (b) Tungsten contribution. The XPS spectrum has been rescaled by a factor of $B = 0.08$. The difference spectrum is compared to the broadened W 5d density of states from the band structure calculation which is shifted by +1 eV to match the experiment.

size seems to depend on details of the calculations (see, for instance, Refs. [38–40]) and is overestimated in our model. The shape of the W 5d spectrum between 3 and 10 eV, however, is comparable for the different band structure approaches. There is a significantly reduced intensity between 3 and 7 eV compared to our experimentally derived result, indicating that the contribution of the tungsten is not appropriately described by the band structure methods. This raises the question about the nature of the intensity that is lacking in the calculations. An indication may be given by the cluster calculation [see Figs. 2 and 4(a)] which shows that it is actually the iron that has spectral features in this energy region. Thus, the spectral weight from the 1-eV region is “transferred” to the 3-7-eV region due to the hybridization with the iron which has inten-

sity there due to correlations that are not captured in the band structure model.

IV. CONCLUSIONS

The photoionization cross-section dependence of the elemental subshells was used to determine the different contributions to the valence band of the Fe²⁺ compound FeWO₄. From the difference of the XPS and HAXPES measurements, we extract the position and shape of the states of the iron and tungsten in the valence band region. A comparison of the experimental results with calculations reveals that the contribution of the iron can be well described by the full atomic multiplet configuration-interaction-based calculation for an octahedral FeO₆ cluster. A calculation of the contribution of the tungsten in a band structure model, however, shows large discrepancies. Although having an empty 5*d* shell, the tungsten states are not well described by a bandlike picture.

This result indicates that the contribution of the tungsten cannot be derived independently by a band structure approach for the FeWO₄ due to an appreciable hybridization of the W 5*d* with the Fe 3*d* mediated by the O 2*p*. One rather has to consider a significantly more complex model with a larger cluster which includes iron as well as tungsten octahedra in the configuration-interaction-based calculation to map the relevant correlation effects.

ACKNOWLEDGMENTS

We thank K. Höfer and C. Becker for skillful technical assistance. We acknowledge J. Falke for advice on the band structure calculations and Z. Hu for fruitful discussions on the electronic structure. The research was supported by the Deutsche Forschungsgemeinschaft through SFB 1143 (Project-ID No. 247310070) and the Max Planck-POSTECH-Hsinchu Center for Complex Phase Materials.

-
- [1] U. M. García-Pérez, A. Martínez-de la Cruz, and J. Peral, Transition metal tungstates synthesized by co-precipitation method: Basic photocatalytic properties, *Electrochim. Acta* **81**, 227 (2012).
- [2] C. M. Gonzalez, X. Du, J. L. Dunford, and M. L. Post, Copper tungstate thin-films for nitric oxide sensing, *Sens. Actuators, B* **173**, 169 (2012).
- [3] P. Chen and H.-Y. He, H₂ evolution from H₂O/H₂O₂/MWO₄ (M = Fe²⁺, Co²⁺, Ni²⁺) systems by photocatalytic reaction, *Res. Chem. Intermed.* **40**, 1947 (2014).
- [4] N. Goubard-Bretesché, O. Crosnier, C. Payen, F. Favier, and T. Brousse, Nanocrystalline FeWO₄ as a pseudocapacitive electrode material for high volumetric energy density supercapacitors operated in an aqueous electrolyte, *Electrochem. Comm.* **57**, 61 (2015).
- [5] J. Liu, Z. Zhang, Z. Wang, M. Tang, J. Li, J. Yi, T. Zuo, Y. Wu, and Q. Ma, Flower-like WO₃/CoWO₄/Co nanostructures as high performance anode for lithium ion batteries, *J. Alloys Compd.* **727**, 107 (2017).
- [6] W. Thongpan, D. Louloudakis, P. Poossekheaw, T. Kumpika, E. Kantarak, W. Sroila, A. Panthawan, W. Thongsuwan, and P. Singjai, Porous CuWO₄/WO₃ composite films with improved electrochromic properties prepared by sparking method, *Mater. Lett.* **257**, 126747 (2019).
- [7] M. J. dos Santos Costa, A. E. B. Lima, E. P. Ribeiro, G. dos Santos Costa, E. Longo, G. E. da Luz, Jr., L. S. Cavalcante, and R. da Silva Santos, Transition metal tungstates AWO₄ (A²⁺ = Fe, Co, Ni, and Cu) thin films and their photoelectrochemical behavior as photoanode for photocatalytic applications, *J. Appl. Electrochem.* **53**, 1349 (2023).
- [8] X. M. C. Ta, T. K. A. Nguyen, A. D. Bui, H. T. Nguyen, R. Daiyan, R. Amal, T. Tran-Phu, and A. Tricoli, Optimizing surface composition and structure of FeWO₄ photoanodes for enhanced water photooxidation, *Adv Mater. Technol.* **8**, 2201760 (2023).
- [9] A. M. Sorouri, A. Sobhani-Nasab, M. R. Ganjali, S. Manani, H. Ehrlich, Y. Joseph, and M. Rahimi-Nasrabadi, Metal tungstates nanostructures for supercapacitors: A review, *Appl. Mater. Today* **32**, 101819 (2023).
- [10] T. Ejima, T. Banse, H. Takatsuka, Y. Kondo, M. Ishino, N. Kimura, M. Watanabe, and I. Matsubara, Microscopic optical and photoelectron measurements of MWO₄ (M = Mn, Fe, and Ni), *J. Lumin.* **119–120**, 59 (2006).
- [11] H. A. Obermayer, H. Dachs, and H. Schröcke, Investigations concerning the coexistence of two magnetic phases in mixed crystals (Fe, Mn)WO₄, *Solid State Commun.* **12**, 779 (1973).
- [12] K. Sieber, K. Kourtakis, R. Kershaw, K. Dwight, and A. Wold, Preparation and photoelectronic properties of FeWO₄, *Mater. Res. Bull.* **17**, 721 (1982).
- [13] R. Guillen and J. R. Regnard, Magnetic properties of natural and synthetic wolframites Fe_xMn_{1-x}WO₄, *Phys. Chem. Miner.* **12**, 246 (1985).
- [14] A. Maignan, M. Schmidt, Y. Prots, O. I. Lebedev, R. Daou, C. F. Chang, C.-Y. Kuo, Z. Hu, C. T. Chen, S.-C. Weng, S. G. Altendorf, L. H. Tjeng, and Y. Grin, FeWO₄ single crystals: Structure, oxidation states, and magnetic and transport properties, *Chem. Mater.* **34**, 789 (2022).
- [15] M. A. P. Almeida, L. S. Cavalcante, C. Morilla-Santos, P. N. Lisboa Filho, A. Beltrán, J. Andrés, L. Gracia, and E. Longo, Electronic structure and magnetic properties of FeWO₄ nanocrystals synthesized by the microwave-hydrothermal method, *Mater. Charact.* **73**, 124 (2012).
- [16] J. Weinen, T. C. Koethe, C. F. Chang, S. Agrestini, D. Kasinathan, Y. F. Liao, H. Fujiwara, C. Schüßler-Langeheine, F. Strigari, T. Hauptrecht, G. Panaccione, F. Offi, G. Monaco, S. Huotari, K.-D. Tsuei, and L. H. Tjeng, Polarization dependent hard x-ray photoemission experiments for solids: Efficiency and limits for unraveling the orbital character of the valence band, *J. Electron Spectrosc. Relat. Phenom.* **198**, 6 (2015).
- [17] A. Fujimori and F. Minami, Valence-band photoemission and optical absorption in nickel compounds, *Phys. Rev. B* **30**, 957 (1984).
- [18] H. Eskes, L. H. Tjeng, and G. A. Sawatzky, Cluster-model calculation of the electronic structure of CuO: A model material for the high-*T_c* superconductors, *Phys. Rev. B* **41**, 288 (1990).
- [19] A. Tanaka and T. Jo, Resonant 3*d*, 3*p* and 3*s* photoemission in transition metal oxides predicted at 2*p* threshold, *J. Phys. Soc. Jpn.* **63**, 2788 (1994).

- [20] K. Koepernik and H. Eschrig, Full-potential nonorthogonal local-orbital minimum-basis band-structure scheme, *Phys. Rev. B* **59**, 1743 (1999).
- [21] J. P. Perdew and Y. Wang, Accurate and simple analytic representation of the electron-gas correlation energy, *Phys. Rev. B* **45**, 13244 (1992).
- [22] X. H. Liu, A. D. Rata, C. F. Chang, A. C. Komarek, and L. H. Tjeng, Verwey transition in Fe_3O_4 thin films: Influence of oxygen stoichiometry and substrate-induced microstructure, *Phys. Rev. B* **90**, 125142 (2014).
- [23] J.-B. Moussy, From epitaxial growth of ferrite thin films to spin-polarized tunnelling, *J. Phys. D: Appl. Phys.* **46**, 143001 (2013).
- [24] T. Yamashita and P. Hayes, Analysis of XPS spectra of Fe^{2+} and Fe^{3+} ions in oxide materials, *Appl. Surf. Sci.* **254**, 2441 (2008).
- [25] Parameters used for the configuration-interaction-based calculation of an octahedral FeO_6 cluster: on-site $3d$ - $3d$ Coulomb energy, $U_{dd} = 5$ eV; charge-transfer energy, $\Delta = 8$ eV; O_h crystal field, $10Dq = 0.6$ eV; hybridization strength between Fe $3d$ and O $2p$, $V_{eg} = 2.36$ eV and $V_{rg} = 1.26$ eV; hybridization strength between O $2p$ orbitals, $T_{pp} = 0.7$ eV; and Slater integrals are 75% of the Hartree-Fock value.
- [26] A. E. Bocquet, T. Mizokawa, T. Saitoh, H. Namatame, and A. Fujimori, Electronic structure of $3d$ -transition-metal compounds by analysis of the $2p$ core-level photoemission spectra, *Phys. Rev. B* **46**, 3771 (1992).
- [27] T. Haupricht, R. Sutarto, M. W. Haverkort, H. Ott, A. Tanaka, H. H. Hsieh, H.-J. Lin, C. T. Chen, Z. Hu, and L. H. Tjeng, Local electronic structure of Fe^{2+} impurities in MgO thin films: Temperature-dependent soft x-ray absorption spectroscopy study, *Phys. Rev. B* **82**, 035120 (2010).
- [28] J.-H. Park, L. H. Tjeng, J. W. Allen, P. Metcalf, and C. T. Chen, Single-particle gap above the verwey transition in Fe_3O_4 , *Phys. Rev. B* **55**, 12813 (1997).
- [29] S. F. Alvarado, M. Erbudak, and P. Munz, Final-state effects in the $3d$ photoelectron spectrum of Fe_3O_4 and comparison with Fe_xO , *Phys. Rev. B* **14**, 2740 (1976).
- [30] T. Fujii, F. M. F. de Groot, G. A. Sawatzky, F. C. Voigt, T. Hibma, and K. Okada, *In situ* XPS analysis of various iron oxide films grown by NO_2 -assisted molecular-beam epitaxy, *Phys. Rev. B* **59**, 3195 (1999).
- [31] T. Saitoh, T. Mizokawa, A. Fujimori, M. Abbate, Y. Takeda, and M. Takano, Electronic structure and temperature-induced paramagnetism in LaCoO_3 , *Phys. Rev. B* **55**, 4257 (1997).
- [32] D. Takegami, A. Tanaka, S. Agrestini, Z. Hu, J. Weinen, M. Rotter, C. Schüßler-Langeheine, T. Willers, T. C. Koethe, T. Lorenz, Y. F. Liao, K. D. Tsuei, H.-J. Lin, C. T. Chen, and L. H. Tjeng, Paramagnetic LaCoO_3 : A Highly Inhomogeneous Mixed Spin-State System, *Phys. Rev. X* **13**, 011037 (2023).
- [33] H. Rosner, J. Gegner, D. Regesch, W. Schnelle, R. Gumeniuk, A. Leithe-Jasper, H. Fujiwara, T. Haupricht, T. C. Koethe, H.-H. Hsieh, H.-J. Lin, C. T. Chen, A. Ormeci, Y. Grin, and L. H. Tjeng, Electronic structure of $\text{SrPt}_4\text{Ge}_{12}$: Combined photoelectron spectroscopy and band structure study, *Phys. Rev. B* **80**, 075114 (2009).
- [34] M. B. Trzhaskovskaya, V. I. Nefedov, and V. G. Yarzhevsky, Photoelectron angular distribution parameters for elements $Z = 1$ to $Z = 54$ in the photoelectron energy range 100–5000 eV, *At. Data Nucl. Data Tables* **77**, 97 (2001).
- [35] M. B. Trzhaskovskaya, V. I. Nefedov, and V. G. Yarzhevsky, Photoelectron angular distribution parameters for elements $Z = 55$ to $Z = 100$ in the photoelectron energy range 100–5000 eV, *At. Data Nucl. Data Tables* **82**, 257 (2002).
- [36] M. B. Trzhaskovskaya, V. K. Nikulin, V. I. Nefedov, and V. G. Yarzhevsky, Non-dipole second order parameters of the photoelectron angular distribution for elements $Z = 1$ –100 in the photoelectron energy range 1–10 keV, *At. Data Nucl. Data Tables* **92**, 245 (2006).
- [37] D. Takegami, L. Nicolai, T. C. Koethe, D. Kasinathan, C. Y. Kuo, Y. F. Liao, K. D. Tsuei, G. Panaccione, F. Offi, G. Monaco, N. B. Brookes, J. Minár, and L. H. Tjeng, Valence band hard x-ray photoelectron spectroscopy on $3d$ transition-metal oxides containing rare-earth elements, *Phys. Rev. B* **99**, 165101 (2019).
- [38] S. Rajagopal, V. L. Bekenev, D. Nataraj, D. Mangalaraj, and O. Y. Khyzhun, Electronic structure of FeWO_4 and CoWO_4 tungstates: First-principles FP-LAPW calculations and X-ray spectroscopy studies, *J. Alloys Compd.* **496**, 61 (2010).
- [39] K. Hoang, Polaron formation, native defects, and electronic conduction in metal tungstates, *Phys. Rev. Mater.* **1**, 024603 (2017).
- [40] R. Schuler, F. Bianchini, T. Norby, and H. Fjellvåg, Near-broken-gap alignment between FeWO_4 and Fe_2WO_6 for ohmic direct p-n junction thermoelectrics, *ACS Appl. Mater. Interfaces* **13**, 7416 (2021).